Behavioral/Cognitive

Language Recovery after Brain Injury: A Structural Network Control Theory Study

Janina Wilmskoetter,[1] Xiaosong He,[2] Lorenzo Caciagli,[2] Jens H. Jensen,[3] Barbara Marebwa,[1] Kathryn A. Davis,[8] Julius Fridriksson,[4] Alexandra Basilakos,[4] Lorelei P. Johnson,[4] Chris Rorden,[5] Danielle Bassett,[2,6,7,8,9,10] and Leonardo Bonilha[1]

[1]Department of Neurology, College of Medicine, Medical University of South Carolina, Charleston, SC 29425, [2]Department of Bioengineering, University of Pennsylvania, Philadelphia, PA 19104, [3]Department of Neuroscience, College of Basic Sciences, Medical University of South Carolina, Charleston, SC 29425, [4]Department of Communication Sciences and Disorders, University of South Carolina, Columbia, SC 29208, [5]Department of Psychology, University of South Carolina, Columbia, SC 29208, [6]Department of Electrical and Systems Engineering, University of Pennsylvania, Philadelphia, PA 19104, [7]Department of Neurology, Perelman School of Medicine, University of Pennsylvania, Philadelphia, PA 19014, [8]Department of Physics & Astronomy, School of Arts & Sciences, University of Pennsylvania, Philadelphia, PA 19014, [9]Department of Psychiatry, Perelman School of Medicine, University of Pennsylvania, Philadelphia, PA 19014, and [10]Santa Fe Institute, Santa Fe, New Mexico, NM 87501

Aphasia recovery after stroke depends on the condition of the remaining, extralesional brain network. Network control theory (NCT) provides a unique, quantitative approach to assess the interaction between brain networks. In this longitudinal, large-scale, whole-brain connectome study, we evaluated whether controllability measures of language-related regions are associated with treated aphasia recovery. Using probabilistic tractography and controlling for the effects of structural lesions, we reconstructed whole-brain diffusion tensor imaging (DTI) connectomes from 68 individuals (20 female, 48 male) with chronic poststroke aphasia who completed a three-week language therapy. Applying principles of NCT, we computed regional (1) average and (2) modal controllability, which decode the ability of a region to (1) spread control input through the brain network and (2) to facilitate brain state transitions. We tested the relationship between pretreatment controllability measures of 20 language-related left hemisphere regions and improvements in naming six months after language therapy using multiple linear regressions and a parsimonious elastic net regression model with cross-validation. Regional controllability of the inferior frontal gyrus (IFG) pars opercularis, pars orbitalis, and the anterior insula were associated with treatment outcomes independently of baseline aphasia severity, lesion volume, age, education, and network size. Modal controllability of the IFG pars opercularis was the strongest predictor of treated aphasia recovery with cross-validation and outperformed traditional graph theory, lesion load, and demographic measures. Regional NCT measures can reflect the status of the residual language network and its interaction with the remaining brain network, being able to predict language recovery after aphasia treatment.

Key words: **aphasia; brain networks; recovery; stroke; white matter**

Significance Statement

Predicting and understanding language recovery after brain injury remains a challenging, albeit a fundamental aspect of human neurology and neuroscience. In this study, we applied network control theory (NCT) to fully harness the concept of brain networks as dynamic systems and to evaluate their interaction. We studied 68 stroke survivors with aphasia who underwent imaging and longitudinal behavioral assessments coupled with language therapy. We found that the controllability of the inferior frontal regional network significantly predicted recovery in language production six months after treatment. Importantly, controllability outperformed traditional demographic, lesion, and graph-theoretical measures. Our findings shed light on the neurobiological basis of human language and can be translated into personalized rehabilitation approaches.

Received May 25, 2021; revised Oct. 20, 2021; accepted Nov. 29, 2021.

Author contributions: J.W. and L.B. designed research; J.W. performed research; C.R. and D.B. contributed unpublished reagents/analytic tools; J.W., X.H., L.C., and B.M. analyzed data; J.W. wrote the first draft of the paper; J.W., X.H., L.C., J.H.J., B.M., K.A.D., J.F., A.B., L.P.J., C.R., D.B., and L.B. edited the paper; J.W. wrote the paper.

This work was supported by National Institutes of Health (NIH)/National Institute of Deafness and Other Communication Disorders Grants DC014021 (to L.B.), U01DC017521 (to L.B.), DC011739 (to J.F.), DC014664 (to J.F.), and T32 DC014435 (to A.B.); the NIH/National Institute of Neurological Disorders and Stroke Grant NS099348-01 (to D.B.); the American Heart Association Grant SFDRN26030003 (to L.B.); American Epilepsy Society (X.H.), John D. and Catherine T. MacArthur Foundation (D.B.); Alfred P. Sloan Foundation (D.B.); and ISI Foundation (D.B.).

The authors declare no competing financial interests.

Correspondence should be addressed to Janina Wilmskoetter at wilmskoe@musc.edu.

https://doi.org/10.1523/JNEUROSCI.1096-21.2021

Introduction

Language is a central aspect of human interaction, and aphasia (language impairment) is associated with severe decrements in quality of life (Wade et al., 1986). Some individuals with chronic aphasia (i.e., lasting more than six months) can significantly improve with language therapy (Wade et al., 1986). However, treatment outcomes are vastly different across individuals. Unfortunately, the underlying neurobiological mechanisms supporting recovery are not fully understood. A better understanding of this problem could help elucidate how the brain adapts to, and recovers from, injury.

It stands to reason that language recovery depends, at least to some extent, on the brain structures preserved after the stroke, particularly on the structural networks integrating these structures. Earlier studies have corroborated the prediction that residual white matter connections are an important factor predicting treated aphasia recovery (Turken and Dronkers, 2011; Baldo et al., 2013; Bonilha et al., 2014a, 2016; Mirman et al., 2015; Dragoy et al., 2017; Pustina et al., 2017; Xing et al., 2017; Meier et al., 2019). For instance, when white matter connecting the inferior frontal cortex or the temporal cortex is damaged after a stroke, aphasia severity and language treatment outcomes are considerably poor, even when these gray matter structures are preserved (Bonilha et al., 2014a, 2016; Gajardo-Vidal et al., 2021). Further, perilesional and associative brain networks have been identified as sites for brain plasticity related to aphasia recovery (Meinzer et al., 2004; Lidzba et al., 2012; McKinnon et al., 2017; Stockert et al., 2020).

However, it remains challenging to understand the complex interactions between residual networks. In this context, recent methodological improvements in the investigation of the neurobiology of neuronal networks may provide further insight. First, using diffusion magnetic resonance imaging (MRI), it is now possible to track mesoscopic and macroscopic pathways across the entire human brain, i.e., the structural brain connectome (Hagmann et al., 2008), and to map the impact of the stroke lesion on the connectome (Gleichgerrcht et al., 2017). Second, mathematical models of complex systems and networks, which have been validated in multiple complex biological systems, can be applied to investigate the brain connectome.

There are multiple approaches to neuronal network modeling (Rubinov and Sporns, 2010). A recently developed framework is network control theory (NCT; Gu et al., 2015). NCT is based on the notion that the brain is a dynamic system transitioning through different activation patterns (brain states) over time. These activation patterns give raise to complex behavioral functions, such as language (Karrer et al., 2020). NCT quantifies brain network properties based on the dynamic interactions of regions with the entire network. NCT provides a computational framework to formalize how functional brain dynamics arise from the underlying network structure (Karrer et al., 2020), and can be applied to neuroscientific inquiry (Gu et al., 2015, 2017; Bernhardt et al., 2019; Karrer et al., 2020). In the context of NCT, a structural brain network is defined as controllable if it is possible to steer such a network into various active "states," defined as coordinated ensembles of neurophysiological activity across brain regions at a specific time point (Karrer et al., 2020). Naturally, specific orchestrations of brain states may subserve different functions or behaviors (Karrer et al., 2020). Based on the structural embedding of a region within the brain network, its ability may differ from other regions to distribute activity through the remaining network, and thus, its ability to influence activity within other regions. Recently, Gu et al. (2015) proposed that cognitive control may be successfully explained by network controllability properties of specific brain regions that could steer the brain network from one state to a target cognitive state. Moreover, Medaglia et al. (2018) demonstrated in healthy individuals a relationship between regional controllability of the inferior frontal gyrus (IFG) and naming performance in open and closed response tasks. This study also demonstrated that regional controllability measures of the IFG explained individuals' change in performance as a response to transcranial magnetic stimulation (TMS) intervention. Thus, prior evidence exists linking regional controllability of the language network to language performance at baseline and as a response to intervention. However, to our knowledge, the application of controllability measures in individuals with stroke is not established. In post-stroke rehabilitation, identifying mechanisms that predict an individual's language performance in chronic stroke and months after treatment is of high clinical importance but remains challenging to this date. In this study, we assessed whether measures of regional controllability of the language network may close this gap of knowledge and provide essential information to predict treated aphasia recovery.

We hypothesized that aphasia recovery depends not only on the number of residual white matter fibers extending to language regions (node strength), but also on the condition (topology) of the residual network. More specifically, we hypothesized that regional network controllability of language related regions would be more strongly associated with recovery than lesion volume, the number of residual white matter connections, or graph theoretical measures of network integration. Should this hypothesis be evinced by the data, it would support the concept that the dynamics of interaction between language regions and the remaining network is an important mechanism underlying recovery.

To test this hypothesis, we examined (1) whether residual brain networks with stroke lesions are controllable in the formal sense of NCT, and (2) whether controllability features of specific regions in the residual language network predict treated language recovery after stroke.

Materials and Methods

We studied data from 74 participants who were part of a Phase II randomized controlled clinical trial (RCT) assessing the role of anodal transcranial direct current stimulation (A-tDCS) as an adjunct to aphasia treatment (Fridriksson et al., 2018a, 2019). The inclusion criteria of the RCT specified that participants must have sustained a one-time stroke in the left-hemisphere. Participants were excluded if they had a history of significant cerebral microangiopathy, dementia, brain surgery, concurrent neurologic disorders, seizures during the previous 12 months, or used medications that lower the seizure threshold. For this study, we further excluded participants with hemorrhagic strokes ($n = 2$) or missing diffusion tensor imaging (DTI) data ($n = 2$). All participants had a chronic ischemic stroke in the left hemisphere, were previously right-handed and were diagnosed with aphasia according to the cutoff for aphasia of the Western Aphasia Battery (Revised; WAB-R; Kertesz, 2007).

In this current study, the main variable of interest is not the effect of tDCS, but the effect of language therapy, which was administered to all participants, regardless of study condition. Participants completed three weeks of computerized language training focused on lexical-semantic processing through a word-picture matching task (Fridriksson et al., 2018a). Participants were seated in front of a computer and instructed to indicate via pressing a green or red button if a spoken word matched with a picture displayed on the computer screen. The spoken words were presented as an audio signal via headphones and as a visual signal displaying the face of the speaker on the computer screen. Immediate feedback was provided whether the participant pressed the correct

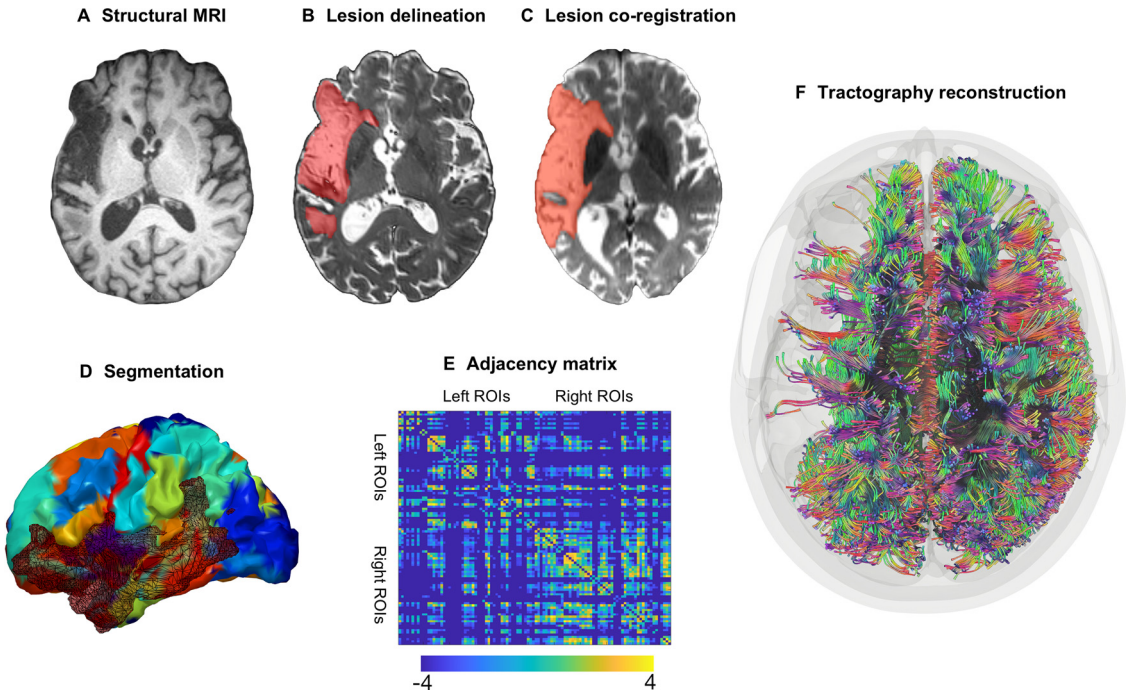

Figure 1. Image processing steps. ***A***, All participants underwent a structural brain MRI scan at baseline. ***B***, Stroke lesions were manually drawn on each participant's T2-weighted image. ***C***, Lesion maps were coregistered to the participant's diffusion-weighted image. ***D***, Each participant's T1-weighted image was segmented into 104 gray matter ROIs with the JHU anatomic atlas; the segmentation maps were registered into diffusion space. ***E***, Probabilistic tractography was computed between every possible gray matter region pair resulting in a 104 × 104 weighted, undirected adjacency matrix where structural connectivity was represented by the (corrected) number of probabilistic streamlines between regions (color bar represent log values for better visualization). ***F***, Visualization of streamlines in brain space (for visualization purposes, this figure is based on deterministic instead of probabilistic tractography).

button. Per session, 160 word-picture pairs were presented of which half were correct, and half contained semantic, phonological, or unrelated foils. Training sessions lasted 45 min and were administered five times a week. Half of the participants were randomized to receive A-tDCS during the first 20 min of language training, while the other half of participants were randomized to receive sham tDCS (S-tDCS) during the first 20 min of language training. Before study enrollment, all participants provided written informed consent. The clinical trial was conducted at the University of South Carolina and the Medical University of South Carolina, whose Institutional Review Boards both approved the study.

Outcome measure for treated aphasia recovery

Our outcome measure was treated anomia recovery, represented by the proportional gains in naming accuracy from before to six months after the aphasia therapy. Naming accuracy was determined based on correct responses on the Philadelphia Naming Test (PNT; Roach et al., 1996). The PNT is a confrontation naming test that includes 175-line drawings depicting nouns of different word lengths and frequencies. The PNT was administered according to the PNT guidelines, twice at baseline and twice on assessment six months after training, to establish reliability of the participants' naming performance. We calculated the average number of correct responses between the two PNTs at baseline and at six-month follow-up. As the dependent variable, we calculated the proportion of maximum gain (PMG) as the percentage of change in naming accuracy from baseline to follow-up, divided by the capacity to improve, as follows:

$$(\text{Avg Correct FU} - \text{Avg Correct BL})/(175 - \text{Avg Correct BL}), \quad (1)$$

where Avg Correct is the average of number of correct responses, FU is the six-month follow-up, and BL is the baseline. Because PMG controls for baseline performance, it accounts to some degree for a variation in the severity of naming impairments across participants. PMG (or similar calculations) have been commonly used in other studies assessing treated aphasia recovery (Lambon Ralph et al., 2010; Gilmore et al., 2019; Kristinsson et al., 2021). Higher values in PMG naming scores denote higher gains in naming accuracy from baseline to follow-up relative to every participant's individual capacity to improve.

Magnetic resonance image acquisition

At baseline, all participants received a structural brain MRI scan on a 3T TIM Trio scanner (Siemens Healthcare) using a 12-channel head coil. We obtained sequences of T1-weighted images [MPRAGE (TFE) sequence: voxel size = 1 mm^3, FOV = 256 × 256 mm^2, sagittal slices = 160, 9° flip angle, TR = 2250 ms, TI = 925 ms, and TE = 4.15 ms], T2-weighted images [3D SPACE (sampling perfection with application optimized contrasts by using different flip angle evolutions): voxel size = 1 mm^3, FOV = 256 × 256 mm^2, sagittal slices = 160, TR = 3200 ms, TE = 212 ms, turbo factor = 129, echo trains per slice = 2, echo train duration = 432 ms], and diffusion tensor weighted images [DTI; twice-refocused EPI sequence: voxel size = 2.7 mm^3, matrix = 82 × 82, TE = 101 ms, TR = 6100 ms, full-Fourier, ×2 GRAPPA in-plane acceleration, 45 contiguous slices without gap, pixel bandwidth = 1355 Hz/px, three different diffusion weighting strengths (b value = 0, 1000, and 2000 s/mm^2) with 30 diffusion-encoding directions, and with two averages within the total 131 volumes acquired (11 b = 0, 60 b = 1000, 60 b = 2000)].

Magnetic resonance image processing

The steps performed in image processing are outlined in shown in Figure 1. Before MRI processing, MR DICOM images were converted to NifTI format using the software dcm2niix (Li et al., 2016).

Lesion delineation

A neurologist and/or trained research specialist manually drew the chronic stroke lesions on each participant's T2-weighted image with the software MRIcron (https://www.nitrc.org/projects/mricron; Fig. 1*B*). Using open source MATLAB scripts that were developed in-house (Rorden et al., 2012), and SPM12 (Functional Imaging Laboratory, Wellcome Trust Center for Neuroimaging Institute of Neurology, University College London; http://www.fil.ion.ucl.ac.uk/spm/software/spm12/), we coregistered the native lesion maps to the participant's

native T1-weighted image and normalized the lesion maps into MNI standard space. For the normalization of the lesion map, we (1) removed uneven edges with a 3-mm full-width at half-maximum Gaussian kernel for smoothing; (2) binarized the smoothed lesion maps (lesioned vs not lesioned tissue) with a threshold of 0; and (3) normalized the T1-weighted image using an enantiomorphic approach (Nachev et al., 2008) onto standard space (chimeric T1-weighted image with a voxel size = 1 mm^3 and with the area corresponding to the stroke lesion being replaced by the mirrored equivalent region in the intact hemisphere) using SPM12's unified segmentation-normalization validated in individuals with a stroke (Rorden et al., 2012).

Structural connectome

The whole-brain probabilistic tractography connectome was extracted for every participant in accordance with previously published methods (Fridriksson et al., 2018b; Wilmskoetter et al., 2019b). Specifically, to segment each participant's normalized T1-weighted image into regions of interest (ROIs; Fig. 1*D*), we used the Johns Hopkins University (JHU) anatomic atlas (Faria et al., 2012), which was applied in previous studies investigating the neuroanatomy of aphasia (Fridriksson et al., 2018b; Wilmskoetter et al., 2019a). From the full set of 189 JHU regions, we focused on 104 gray matter areas (for a list of all regions, see Table 1). We registered the gray matter JHU segmentation maps to the DTI space and computed probabilistic tractography between every possible pair of gray matter region. First, we removed distortions in the diffusion images using eddy current correction (Andersson and Sotiropoulos, 2016). All diffusion images were acquired with the same phase encoding polarity, and distortions in the acquired images were reduced with twice-refocused sequences and in-plane accelerations (Reese et al., 2003). Second, we computed tractography using the probabilistic method of FSL's FMRIB's Diffusion Toolbox (Behrens et al., 2007) with the toolbox's accelerated BEDPOST (Hernández et al., 2013) and probtrackX with 5000 individual pathways, drawn through probability distributions on principal fiber direction, curvature threshold = 0.2, maximum steps = 200, step length = 0.5 mm, and distance correction. The stroke lesion was excluded from tractography. We obtained the weighted connectivity link for a pair of regions A and B by averaging the number of probabilistic streamlines from A to B and from B to A. We corrected the weighted connectivity links for every streamline's distance between A and B (or B and A) for the size of region A and the size of region B (Gross, 2008; Bonilha et al., 2015). As a result, every connectome consisted of a 104 × 104 matrix (Fig. 1*E*). In this network, the nodes represent the 104 JHU gray matter regions and edges represent the weighted connectivity links.

To exclude links with low probability, links whose weights were below the lowest 20% percentile of the links in the right unlesioned hemisphere were set to zero (Mirman et al., 2015). We calculated the percentage of links set to zero for the final cohort of 68 participants. As explained in more detail below, two more of the 70 participants were later excluded based on lack of controllable brain networks. Across the 68 participants on average 23.6% (SD 7.0%) of links were set to zero. When adding all other links that were zero, on average 55.3% (SD 10.3%) of all links in the entire brain had a weight of zero. In conclusion, for each participant, a 104 × 104 weighted undirected adjacency matrix representing structural connectivity was obtained.

MRI analyses

We calculated network controllability of every participant's individual structural connectome by using previously described methods (Gu et al., 2015). We first determined whether a participant's connectome is controllable, and second, calculated controllability diagnostics, i.e., average controllability and modal controllability. The steps are described below.

Global controllability

Controllability refers to the possibility to move the dynamical brain network into a target state by changing a single brain region's activity using external input energy. Thus, a network is not controllable if there are target states that cannot be reached by controlling any brain region independently of its input energy (Karrer et al., 2020).

To ensure a valid application of controllability measures to a network, the network itself needs to be controllable. The controllability of a network is determined by (1) the energy applied to the network, and by (2) the connectivity links of the network. If regions within a network are not connected to the remaining network, it is impossible that these regions can control the network regardless of how much energy is applied to the region. In the case of brain networks with a lesion, as in the participants with a history of stroke, some regions can be disconnected, at least in terms of white matter, from the remaining network and thus, may not be able to control the whole network. Therefore, on a case-by-case basis, we excluded all regions with no white matter connection to another region (zero-degree nodes) from each participant's network and assessed whether participants' residual connectomes were controllable by calculating a measure of global controllability. Seeding one brain region (node) at a time (for up to 104 regions, depending on how many zero-degree nodes were excluded), we computed the controllability Gramian for each node using the entire connectome matrix as input (size of the matrix was up to 104 × 104). If the smallest eigenvalue across all controllability Gramians was >0, the participant's structural connectome was considered controllable (Gu et al., 2015; Karrer et al., 2020).

Regional controllability

Our second objective was to determine whether controllability features of specific regions in the residual language network predict treated language recovery after stroke. To examine this, we analyzed regional controllability by calculating average controllability and modal controllability for every brain region in participants who had a controllable structural connectome. Average and modal controllability describe two distinct nodal properties for control goals. In a controllable network, the magnitudes of average and modal controllability can be computed for every region and in brain networks are typically inversely proportional (Gu et al., 2015; Karrer et al., 2020); thus, a node with high average controllability generally exhibits low modal controllability.

Average controllability quantifies the energetical response of the brain system to a regional impulse (control input) and describes a region's ability to spread and amplify the energy of the control input through the remaining network (Karrer et al., 2020). If regions with high average controllability receive control input, the larger and more widespread is the response of the remaining brain system. As a result, for regions with high average controllability less input energy is required to control this region and more target states can be reached. Thus, average controllability describes the efficiency of a region in supporting brain state transitions by spreading and amplifying energy throughout the brain. Brain regions with high average controllability can be interpreted as "hub" regions, that are highly connected to the remaining network and have high network degree values. Among healthy individuals, regions with high average controllability include the precuneus, superior frontal, posterior cingulate and subcortical regions (Gu et al., 2015; Karrer et al., 2020). Average controllability was calculated as $Trace(W_K)$, where W refers to the controllability Gramian of a participant's connectome, and K indexes nodes in the connectome.

Modal controllability quantifies a region's ability to control all possible brain states. Energy injected into a region with high modal controllability allows for more diverse state transitions. In contrast to average controllability, brain regions with high modal controllability are sparsely connected to the remaining network and have low degree. Examples of regions with high modal controllability among healthy individuals include the postcentral gyrus, supramarginal gyrus, and IFG pars orbitalis (Gu et al., 2015). Modal controllability was calculated from the eigenvalues λj and the normalized eigenvector matrix $V=[v_{i,j}]$ of the connectome matrix, where i represents a brain region (node) and λj a brain state (Karrer et al., 2020). Therefore, modal controllability is a measure of node's i ability to control brain state j and corresponds to the projection of node i onto eigenvector j.

For statistical comparisons between participants, we normalized the regional controllability values for every participant by calculating the rank of each node across the entire set of 104 nodes in each participant's connectome. Zero-degree nodes were assigned the lowest ranks.

Table 1. List of gray matter regions selected from the Johns Hopkins University (JHU) anatomic atlas

Left hemisphere			Right hemisphere	
Region group	Region label	Region from JHU anatomic atlas	Region label	Region group
Left frontal	SFG_L	Superior frontal gyrus (posterior segment)	SFG_R	Right frontal
	SFG_PFC_L	Superior frontal gyrus (prefrontal cortex)	SFG_PFC_R	
	SFG_pole_L	Superior frontal gyrus (frontal pole)	SFG_pole_R	
	MFG_L*	Middle frontal gyrus (posterior segment)	MFG_R	
	MFG_DPFC_L	Middle frontal gyrus (dorsal prefrontal cortex)	MFG_DPFC_R	
	IFG_opercularis_L*	Inferior frontal gyrus pars opercularis	IFG_opercularis_R	
	IFG_orbitralis_L*	Inferior frontal gyrus pars orbitralis	IFG_orbitralis_R	
	IFG_triangularis_L*	Inferior frontal gyrus pars triangularis	IFG_triangularis_R	
	LFOG_L	Lateral fronto-orbital gyrus	LFOG_R	
	MFOG_L	Middle fronto-orbital gyrus	MFOG_R	
	RG_L	Rectus gyrus	RG_R	
	PrCG_L*	Precentral gyrus	PrCG_R	
	rostral_ACC_L	Rostral anterior cingulate gyrus	rostral_ACC_R	
	subcallosal_ACC_L	Subcallosal anterior cingulate gyrus	subcallosal_ACC_R	
	subgenual_ACC_L	Subgenual anterior cingulate gyrus	subgenual_ACC_R	
	dorsal_ACC_L	Dorsal anterior cingulate gyrus	dorsal_ACC_R	
Left insula	Ins_L*	Anterior insula	Ins_R	Right insula
	PIns_L*	Posterior insula	PIns_R	
Left temporal	STG_L*	Superior temporal gyrus	STG_R	Right temporal
	STG_L_pole*	Pole of superior temporal gyrus	STG_R_pole	
	MTG_L*	Middle temporal gyrus	MTG_R	
	MTG_L_pole*	Pole of middle temporal gyrus	MTG_R_pole	
	ITG_L*	Inferior temporal gyrus	ITG_R	
	PHG_L	Parahippocampal gyrus	PHG_R	
	ENT_L	Entorhinal area	ENT_R	
	FuG_L	Fusiform gyrus	FuG_R	
	Amyg_L	Amygdala	Amyg_R	
	Hippo_L	Hippocampus	Hippo_R	
	PSTG_L*	Posterior superior temporal gyrus	PSTG_R	
	PSMG_L*	Posterior middle temporal gyrus	PSMG_R	
	PSIG_L	Posterior inferior temporal gyrus	PSIG_R	
Left subcortical	Caud_L	Caudate nucleus	Caud_R	Right subcortical
	Put_L*	Putamen	Put_R	
	GP_L*	Globus pallidus	GP_R	
	Thal_L	Thalamus	Thal_R	
	Hypothalamus_L	Hypothalamus	Hypothalamus_R	
	Mynert_L	Nucleus innominata of mynert	Mynert_R	
	NucAccumbens_L	Nucleus accumbens	NucAccumbens_R	
Left Parietal	PoCG_L*	Postcentral gyrus	PoCG_R	Right parietal
	SPG_L	Superior parietal gyrus	SPG_R	
	SMG_L*	Supramarginal gyrus	SMG_R	
	AG_L*	Angular gyrus	AG_R	
	PrCu_L	Precuneus	PrCu_R	
	PCC_L	Posterior cingulate gyrus	PCC_R	
Left occipital	SOG_L	Superior occipital gyrus	SOG_R	Right occipital
	MOG_L*	Middle occipital gyrus	MOG_R	
	IOG_L	Inferior occipital gyrus	IOG_R	
	Cu_L	Cuneus	Cu_R	
	LG_L	Lingual gyrus	LG_R	

Regions on the left side of the circular diagrams of Figure 6 correspond in counterclockwise order to regions listed from top to bottom in this table. Likewise, regions on the right side of the circular diagrams correspond in clockwise order to regions listed from top to bottom in this table. Because of visualization purposes substantia nigra, red nucleus and mammillary body are not displayed in the circular diagrams or listed in this table. JHU = Johns Hopkins University. * denote regions that were included in the set of 20 language-related left hemisphere gray matter regions.

Selection of language-related regions

To determine whether regional controllability within the language network is associated with treated aphasia recovery, we selected 20 language-related left hemisphere gray matter regions, based on previous literature on critical language-related regions supporting aphasia recovery (Fridriksson et al., 2016): IFG pars triangularis, pars orbitalis, pars opercularis, middle frontal gyrus, precentral gyrus, postcentral gyrus, supramarginal gyrus, angular gyrus, superior temporal gyrus (pole, middle, and posterior part), middle temporal gyrus (pole, middle, and posterior part), inferior temporal gyrus, anterior and posterior insula, middle occipital gyrus (MOG), putamen, and globus pallidus.

We focused on the language network in the left hemisphere because current research suggests that, for individuals who exhibit left-hemisphere language dominance, language recovery after a stroke relies on the reorganization of language specific residual brain networks in the left hemisphere (Stockert et al., 2020) and, further, that the language network itself may only receive little input from other domain-general executive control networks (Shain et al., 2020).

Other imaging control variables: graph theory measures and regional lesion load

Because regional controllability measures are calculated based on structural network properties and may share some similarities with

traditional graph theory measures (Gu et al., 2015), we compared the predictive value for aphasia recovery of both measurement types. We calculated established regional (local) graph theory measures (node strength, node betweenness centrality) as well as regional lesion load (calculated as the percentage of lesion in a region) to determine how these measures relate to regional controllability (average and modal controllability). Previous work has shown that controllability diverges from other graph measures in ways that are reflective of the complexity of regional computations (Parkes et al., 2020). Demonstrating additional insights from controllability measures beyond information conveyed by traditional graph theory and regional lesion load measures would provide further support to their use in future studies on post-stroke aphasia.

We used the Brain Connectivity Toolbox to compute node strength and betweenness centrality (Rubinov and Sporns, 2010). Node strength was calculated for each node as the sum of undirected weighted links connected to a given node. Node betweenness centrality for a region (B_k) was calculated for each node as the proportion of shortest paths between regions i and j that pass through node k (Brandes, 2001). For normalization purposes, we computed the rank of each node across the entire set of 104 nodes in each participant's connectome (Gu et al., 2015). A node with a higher number of shorter path connections to the remaining network can more easily influence the state of the network.

Statistical analyses

We performed explanatory and predictive statistical modeling to assess whether regional controllability is associated with treated aphasia recovery, and whether it aides out of sample predictions, respectively.

For explanatory modeling, we applied multivariable linear regression to assess whether regional controllability of any of the 20 language regions is associated with the outcome variable "PMG naming score" while controlling for regional controllability of the remaining 19 ROIs. We performed two different linear regression models, one for average controllability and one for modal controllability: (1) dependent variable: PMG naming score; primary independent variables: average controllability of each of the 20 language-related regions; and (2) dependent variable: PMG naming score; primary independent variables: modal controllability of each of the 20 language-related regions.

In both models, we controlled for baseline aphasia severity (WAB-AQ), education, age, therapy type (A-tDCS vs S-tDCS), total lesion volume, and number of edges (global degree). By controlling for the number of edges, we sought to control for any differences in network size across participants. We excluded independent variables if they showed high multicollinearity, as indicated by a variance inflation factor >6.

After explanatory modeling, we performed predictive statistical modeling to test whether controllability measures support generalizability to nontraining samples, assessing whether controllability measures outperform traditional graph theory and regional lesion load measures in predicting treated aphasia recovery. Therefore, we applied elastic net regression modeling with cross-validation to build a parsimonious predictive model (Zou and Hastie, 2005). Elastic net regularization combines lasso and ridge regularization penalties to select a set of predictors from a pool of candidate predictors that provides the highest predictive value for an outcome measure (in this study, PMG naming score). Elastic net modeling is especially useful in situations with more predictors than observations, and highly multicollinear predictors. We performed regularization from zero (min) to one (max) in increments of 0.1 for ridge and 0.02 for lasso penalties. Ten-fold cross-validation was applied (convergence criterion: 0.00001 with max. 100 iterations). The set of candidate independent variables included a total of 106 variables: average controllability, modal controllability, node strength, node betweenness centrality, lesion volume for each of the 20 nodes, and age, education, baseline WAB-AQ, therapy type (A-tDCS vs S-tDCS), total lesion volume, and number of edges.

Two-tailed statistical tests were used, and $p < 0.05$ was considered statistically significant. MATLAB (version R2019b, 9.7.0.1140744, released 2019, The MathWorks Inc.) and IBM SPSS Statistics for Windows (version 25, released 2017, IBM Corp.) were used to conduct all statistical analyses.

Results

Outcome measure for treated aphasia recovery

A related-samples Wilcoxon signed-rank test showed that the room to improve changed significantly from baseline to six-month follow-up ($Z = 456$, $p < 0.001$). Participants had a median room to improve of 120.75 at baseline, and a median room to improve of 114.00 at six-month follow-up. Thus, overall, the treatment intervention resulted in a significant improvement in correct naming responses.

Global controllability

Sixty-eight of the 70 participants with ischemic strokes had connectomes that were controllable from every single region. The smallest eigenvalues of the controllability Gramians were >0 for all remaining 68 participants (mean 9.05×10^{-27}, SD 3.73×10^{-26}). Please refer to Figure 2*A* and Table 2 for lesion characteristics, demographic and clinical information related to the 68 participants included in the final analyses. While the participants varied in their stroke chronicity ranging from six months to 16 years, the time since stroke did not relate to the PMG naming score (Spearman's $\rho = -0.07$, $p = 0.57$).

An average of 2.5 regions (median: 2, range: 0–16) were excluded across participants as zero-degree nodes (Fig. 2*B* shows the regions with zero-degree nodes). For example, in seven participants the IFG pars opercularis was a zero-degree node, and thus was excluded from the connectome of these participants. Note that these participants were not excluded from the statistical analyses, which included controllability of IFG pars opercularis as well as the degree. More specifically, this step did not bias the analyses toward finding a relationship between aphasia and a region's controllability, with regional controllability serving as a proxy for lesion. Lesion volume was included in all analyses as a separate variable.

Likewise, the spatial distribution of zero-degree nodes did not mirror the lesion overlay (Fig. 2*A*). While the pole of the left superior frontal gyrus was most commonly disconnected from the remaining network, being a zero-degree node in 25 of the 68 participants; it was lesioned in only one participant. The posterior superior temporal gyrus was lesioned in 46 participants (on average 60% lesion across all participants) but was disconnected from the remaining network in only four of the 68 participants. The statistical models also included lesion volume for the same reason.

Regional controllability

Figure 2*C*,*D* show the median rank for each of the 20 language-related nodes for average and modal controllability, respectively. The left MOG had the highest average controllability within the language network, with a rank of 73 across all 104 gray matter regions. The left anterior insula had the lowest average controllability (rank 20). The left anterior insula had the highest (rank 73) and the left posterior middle temporal gyrus had the lowest (rank 30) modal controllability within the language network. In line with previous evidence in brain networks, average and modal controllability have opposite directions (Gu et al., 2015; Karrer et al., 2020), where regions with high average controllability are more likely to have low modal controllability and vice versa. We found no association between average or modal controllability with node strength or node betweenness centrality for the 20 selected language-related ROIs but found weak to moderate associations between average or modal controllability and regional lesion volume (Fig. 3). The left MOG left anterior insula and left posterior middle temporal gyrus had on average the

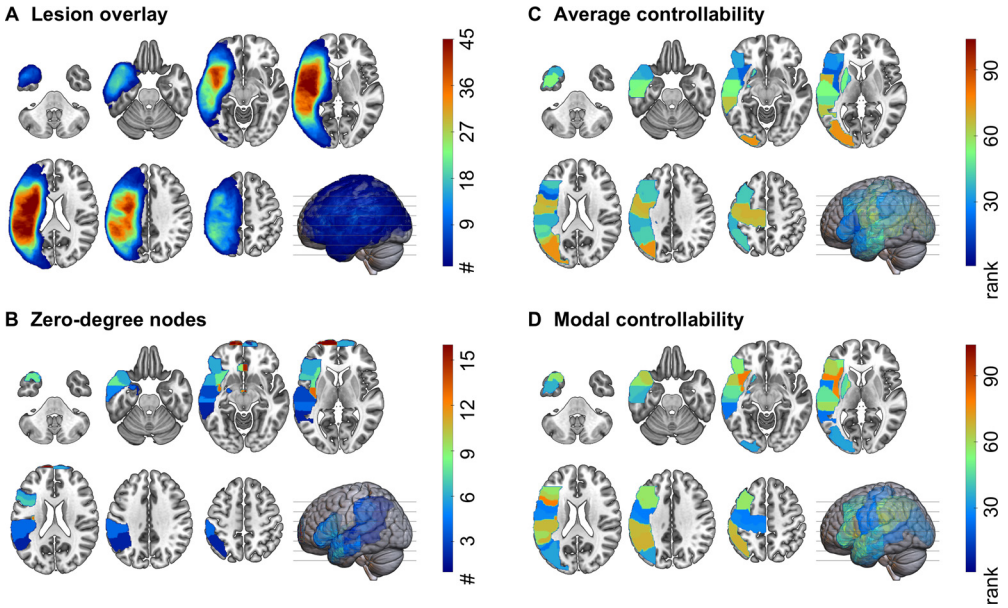

Figure 2. Lesion and regional characteristics. ***A***, Lesion overlay of all participants included in the final analyses ($n = 68$). Different numbers of participants with a lesion in an area are represented by different colors. The more participants shared a lesion in an area, the warmer the color. As expected, most participants had lesions around the sylvian fissure. ***B***, Zero-degree nodes (brain areas disconnected from the remaining network) across all participants. The more participants shared a zero-degree node in that area, the warmer the color. ***C***, ***D***, Regional controllability of the 20 left hemisphere language-related ROIs included in this study. The controllability values were ranked across all 104 gray matter regions. The visualizations in this figure show the average (median) ranks across all participants. The warmer the color, the higher the value of average (***C***) or modal (***D***) controllability. Note that average and modal controllability are in general inversely related: nodes with higher average controllability tend to have lower modal controllability, and vice versa.

Table 2. Demographic and diagnostic information of all participants included in the final analyses ($n = 68$)

Demographic information		
Age, mean (SD; range)	59.7 (10.2; 30–77)	
Sex, *n* (%)	Female	20 (29.4)
	Male	48 (70.6)
Race, *n* (%)	White	56 (82.3)
	African American	10 (14.7)
	Asian	2 (3.0)
Education (highest year of school completed); years, mean (SD; range)		14.8 (2.4; 10–20)
Diagnostic information		
Years since stroke, mean (SD; range)		3.4 (3.3; 0.5–16.9)
WAB-AQ (max. 100), mean (SD; range)		59.0 (19.5; 27.8–93.7)
Average correct responses in the 2 PNTs at baseline (max. 175), mean (SD; range)		60.8 (43.4; 0.5–139)
Average change in correct responses in the 2 PNTs from baseline to 6 months after therapy (max. 175), mean (SD; range)		6.6 (14.6; −32–52.5)

n = number; PNT = Philadelphia Naming Test (Roach et al., 1996); WAB-AQ = Aphasia Quotient of the Western Aphasia Battery (Revised; Kertesz, 2007).

28th, 4th, and 10th greatest lesion burden across all 104 regions, respectively.

Explanatory multivariable regression modeling

Average controllability

Using multivariable linear regression modeling, average controllability of IFG pars opercularis was significantly associated with PMG naming scores ($\beta = 0.39$, $p = 0.038$), independently of the average controllability of any other language region, baseline aphasia severity, education, age, therapy type, total lesion volume, and number of edges; the higher the average controllability of IFG pars opercularis, the better the naming gains (Fig. 4*A*). Average controllability of no other region and no other control variable was statistically significant (Table 3).

Modal controllability

Modal controllability of the IFG pars orbitalis and anterior insula were significantly associated with PMG naming scores ($\beta = -0.34$, $p = 0.033$ and $\beta = 0.36$, $p = 0.036$, respectively), with lower modal controllability of the IFG pars orbitalis (Fig. 4*B*) and higher modal controllability of the anterior insula (Fig. 4*C*) being associated with higher improvement in naming performance after therapy. In the same model, WAB-AQ at baseline was significantly associated with PMG naming scores ($\beta = 0.38$, $p = 0.047$), with higher WAB-AQs (less severe aphasia) being associated with better improvement (Table 4).

Relationship between stroke lesions and regional controllability

As expected, the number of zero-degree nodes was strongly associated with the total brain lesion volume (Pearson's $r = 0.59$; $p < 0.001$; Fig. 5). The ranked average controllability of the IFG pars opercularis was significantly correlated with the IFG pars opercularis regional lesion volume (Pearson's $r = -0.59$; $p < 0.001$) and with the total brain lesion volume (Pearson's $r = -0.33$; $p = 0.005$), but not with its ranked node strength (Pearson's $r = -0.04$; $p = 0.77$) or ranked betweenness centrality

Table 3. Multiple linear regression model to assess the influence of average controllability on the outcome PMG naming scores from baseline to 24 weeks (six months) after therapy with an overall model fit of $R^2 = 0.31$

Variable		β	SE β	β	p
Intercept	0.053	0.310		0.864	
Average controllability	Pars opercularis	0.004	0.002	0.391	0.038*
	Precentral gyrus	<−0.001	0.002	−0.002	0.992
	Supramarginal gyrus	−0.001	0.002	−0.131	0.609
	Angular gyrus	<0.001	0.002	0.060	0.817
	Pole of superior temporal gyrus	<0.001	0.003	−0.043	0.855
	Pole of middle temporal gyrus	0.001	0.003	0.060	0.831
	Middle occipital gyrus	0.002	0.002	0.175	0.445
	Anterior insula	−0.001	0.003	−0.055	0.779
	Putamen	−0.003	0.002	−0.249	0.239
	Posterior insula	0.003	0.002	0.282	0.232
	Posterior superior temporal gyrus	−0.002	0.002	−0.280	0.251
	Posterior middle temporal gyrus	−0.001	0.002	−0.280	0.715
WAB-AQ baseline		0.002	0.002	0.223	0.191
Age		−0.005	0.003	−0.274	0.128
Education		0.007	0.011	0.095	0.519
Therapy type (A-tDCS vs S-tDCS)		0.061	0.052	0.171	0.246
Total lesion volume		<−0.001	0	−0.113	0.636
Number of edges		<0.001	0	0.168	0.388

β = standardized regression coefficient; *significant at the α level $p < 0.05$.

Table 4. Multiple linear regression model to assess the influence of modal controllability on the outcome PMG naming scores from baseline to 24 weeks (six months) with an overall model fit of $R^2 = 0.44$

Variable		β	SE β	β	p
Intercept	0.181	0.379		0.636	
Modal controllability	Middle frontal gyrus	−0.001	0.001	−0.099	0.560
	Pars opercularis	0.001	0.001	0.160	0.415
	Pars orbitalis	−0.002	0.001	−0.343	0.033*
	Pars triangularis	−0.001	0.001	−0.194	0.296
	Postcentral gyrus	−0.003	0.002	−0.358	0.143
	Supramarginal gyrus	−0.001	0.001	−0.165	0.380
	Angular gyrus	0.001	0.001	0.221	0.225
	Superior temporal gyrus	0.002	0.002	0.222	0.310
	Pole of superior temporal gyrus	<0.001	0.001	−0.023	0.889
	Middle temporal gyrus	<0.001	0.001	−0.062	0.756
	Pole of middle temporal gyrus	<0.001	0.001	−0.061	0.706
	Inferior temporal gyrus	<0.001	0.001	−0.064	0.763
	Middle occipital gyrus	−0.002	0.002	−0.257	0.156
	Anterior insula	0.002	0.002	0.359	0.036*
	Globus pallidus	<0.001	0.002	0.013	0.934
	Posterior insula	<0.001	0.001	−0.034	0.832
	Posterior superior temporal gyrus	−0.001	0.001	−0.104	0.529
	Posterior middle temporal gyrus	<0.001	0.001	0.050	0.811
WAB-AQ baseline		0.003	0.002	0.377	0.047*
Age		−0.005	0.003	−0.276	0.116
Education		0.016	0.010	0.216	0.139
Therapy type (A-tDCS vs S-tDCS)		0.045	0.052	0.126	0.392
Total lesion volume		<0.001	<0.001	0.093	0.719
Number of edges		<−0.001	<0.001	−0.122	0.528

β = standardized regression coefficient; *significant at the α level $p < 0.05$.

(Pearson's $r = 0.06$; $p = 0.64$). The ranked modal controllability of the IFG pars orbitalis was correlated with the IFG pars orbitalis' regional lesion volume (Pearson's $r = 0.29$; $p = 0.02$), but not with the total brain lesion volume (Pearson's $r = -0.02$; $p = 0.82$), ranked node strength (Pearson's $r = -0.05$; $p = 0.71$), or ranked betweenness centrality (Pearson's $r = -0.05$; $p = 0.70$). The ranked modal controllability of the anterior insula was not significantly correlated with any measure (total lesion volume: Pearson's $r = -0.22$; $p = 0.07$; own regional lesion volume: Pearson's $r = -0.20$; $p = 0.10$; ranked node strength: Pearson's $r = -0.13$; $p = 0.29$; ranked betweenness centrality: Pearson's $r = -0.01$; $p = 0.97$).

Elastic net prediction modeling

Elastic net prediction modeling was used to determine whether regional controllability aides in out-of-sample prediction. This step was not aided, informed, or modified based on the regression analyses described above. We did not choose the variables that were included in the final prediction model. All 106 variables, 40 of which were measures of regional controllability, were used as candidate predictors, with the intent of validating and confirming the findings from the explanatory models without biasing the predictive model.

With elastic net modeling using 10-fold cross validation, two out of 106 candidate variables were retained in the optimal model to predict PMG naming scores: (1) average controllability of IFG pars opercularis ($\beta = 0.27$), and (2) baseline WAB-AQ ($\beta = 0.22$). The model had an overall fit of $R^2 = 0.156$, and an expected prediction error estimate (10-fold cross-validation) of 1.12 (SD = 0.19). In *post hoc* linear regression analyses, we assessed the predictive value of average controllability independent from baseline aphasia severity. We extracted the residuals of average controllability of IFG pars opercularis by regressing baseline WAB-AQ. In a simple linear regression model, the residuals from average controllability of IFG pars opercularis significantly predicted PMG naming scores ($\beta = 0.26$, $p = 0.038$).

Discussion

In this study, we observed that inferior frontal and insular regional network controllability, based on residual poststroke white matter network topology, significantly predicted individualized treated language recovery in a cohort of participants undergoing aphasia treatment. Regional network controllability outperformed traditional demographic, lesion, and graph-theoretical measures. These results provide an important first step toward the understanding of the network mechanisms underlying language dysfunction. Importantly, this study did not assess neurophysiological brain states that each participant's network can transition to, i.e., patterns of brain activation explaining language recovery. Instead, we focused on the initial and necessary evaluation of whether topological properties of the residual networks, quantified from a NCT standpoint, are associated with, and are predictive of, aphasia recovery. The implications of these findings are discussed below.

Most brain networks with stroke lesions are controllable

We observed that 97% of the individual brain connectomes (68 of 70) were controllable, taking into account the zero-degree nodes within the lesion, or outside of the lesion because of reduced connectivity, possibly as a result of small vessel disease and white matter injury preceding the stroke (Wilmskoetter et al., 2019b), or deafferentation from the stroke lesion (Bonilha et al., 2014b). Additional explanations may relate to technical aspects, including the inability to resolve crossing fibers or complex fiber anatomy poststroke via diffusion MRI, or reduced sensitivity to partially gliotic regions.

While we observed that the connectomes of most participants were controllable, the magnitude of global controllability was low, indicating that the energy needed to change the state of the

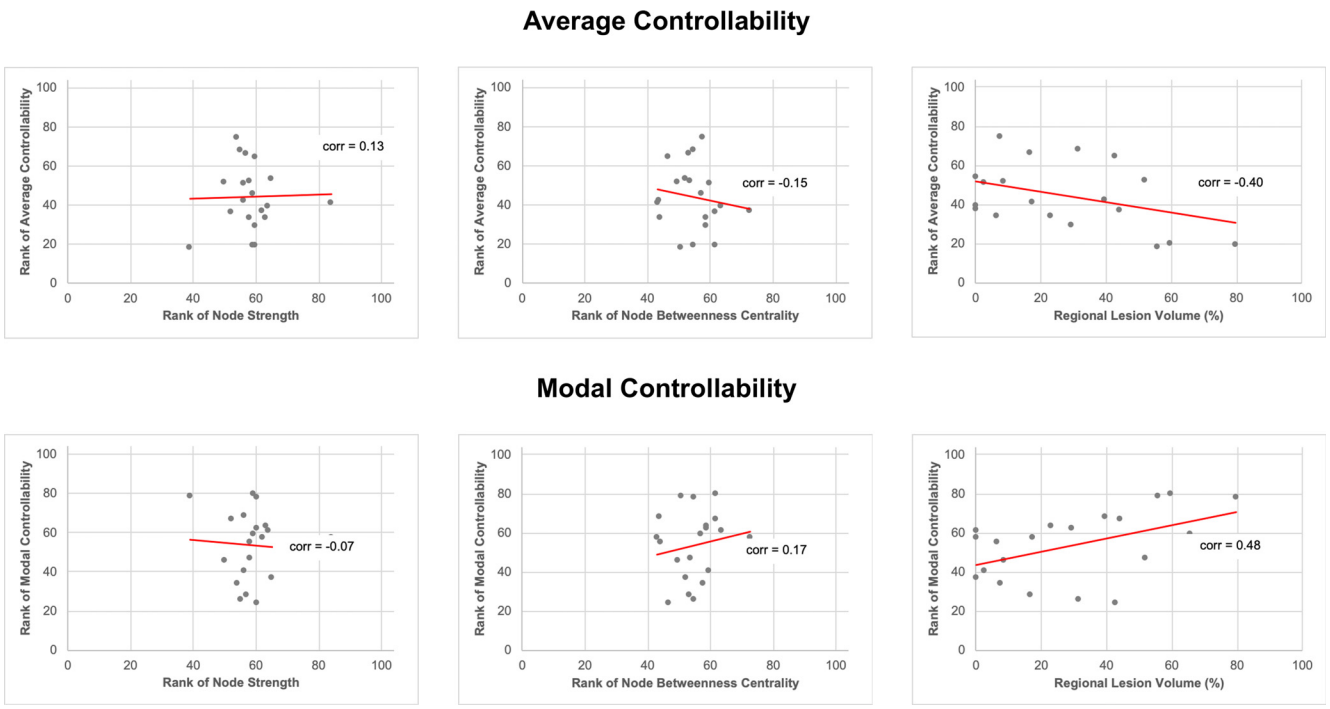

Figure 3. Scatter plots of regional controllability measures versus local graph theory measures and regional lesion volume for all 20 language-related regions. The median was obtained for all variables (for each region across all 68 participants). Regional controllability measures (average and modal controllability) and local graph theory measures (node degree, node betweenness centrality) were ranked across all 104 gray matter regions, but only the 20 language-related regions are displayed here. Note that average and modal controllability did not correlate with node degree or betweenness centrality (|Spearman's $\rho| < 0.20$, $p > 0.05$), but did correlate weakly with regional lesion volume (|Spearman's $\rho| > 0.4$, $p < 0.05$). corr = Spearman's ρ.

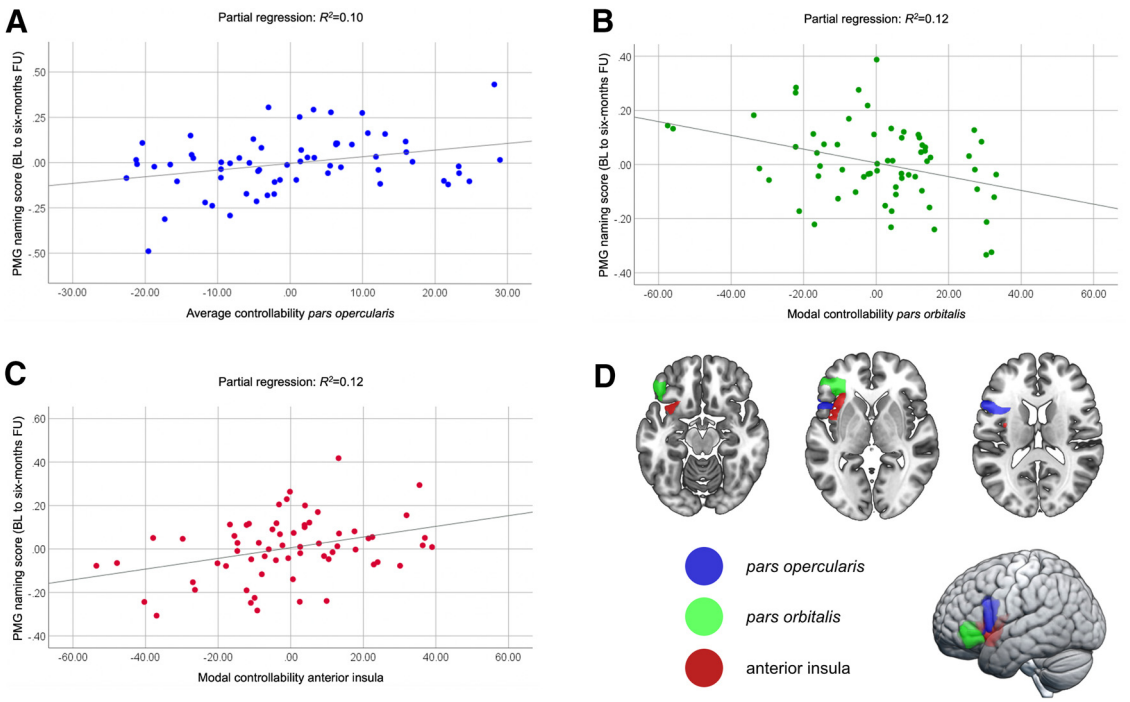

Figure 4. Explanatory multivariable regression modeling. Scatter plots for the partial regression of (***A***) average controllability of the IFG pars opercularis, (***B***) modal controllability of the IFG pars orbitalis, and (***C***) modal controllability of the anterior insula in explaining PMG naming scores from baseline (BL) to six-month follow-up (FU) after therapy. ***D***, Anatomical locations of the IFG pars opercularis (blue), IFG pars orbitalis (green), and anterior insula (red).

brain from a single region is substantial. This observation is not specific to structural connectomes with stroke lesions but was also observed in studies that applied NCT to structural connectomes in healthy adults (Gu et al., 2015). Thus, controlling the entire brain from one single region is theoretically possible, but may require impractically high levels of energy. Importantly, this finding does not preclude the clinical application of NCT to patients with stroke, as demonstrated by this study and by a

previous study that successfully explained the effects of neuromodulation on language performance in healthy adults via regional controllability features (Medaglia et al., 2018). Of note, it is important to consider global network controllability in the context of language processing, i.e., language processing may not require input from all regions or to all regions and may be mostly limited to a confined network of language-specific regions (Shain et al., 2020).

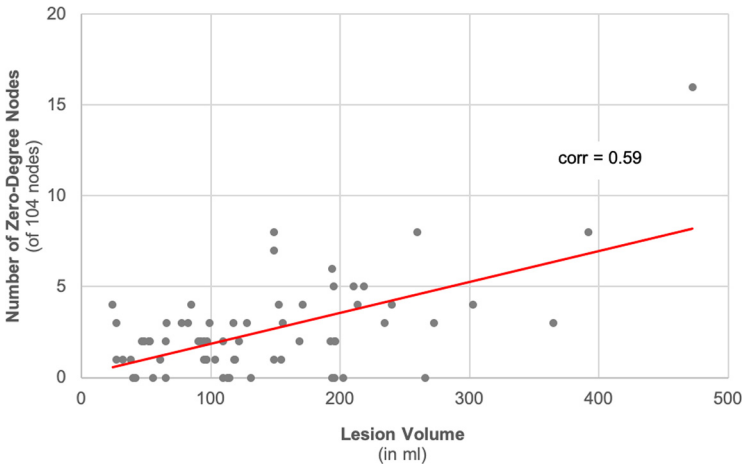

Figure 5. Scatter plot of total brain lesion volume versus number of zero-degree nodes. Zero-degree nodes were calculated across all 104 gray matter anatomic regions. The number of zero-degree nodes was overall related to the total brain lesion volume (Pearson correlation coefficient = 0.59; $p < 0.001$). corr = Pearson correlation coefficient.

Regional controllability, residual network interaction, and language recovery

We found evidence that controllability features of specific regions in the residual language network after stroke were associated with and predicted treated language recovery six months after treatment. Higher average controllability of the left IFG pars opercularis, lower modal controllability of the left IFG pars orbitalis, and higher modal controllability of the left anterior insula were associated with higher improvement in naming accuracy after therapy. Because of the typically inverse relationship between average and modal controllability (Gu et al., 2015; Karrer et al., 2020), nodes with high average controllability usually have low modal controllability. Our findings suggest that both sections of the IFG, pars orbitalis and opercularis can be drivers of aphasia recovery based on their structural connectivity pattern that supports their dynamic interaction with the remaining network.

The importance of high average controllability of the IFG was further supported by our elastic net regression approach, that provided a parsimonious model with the highest possible out-of-trained-sample predictive value. Average controllability of the left IFG pars opercularis was selected as a crucial predictor alongside baseline aphasia severity. Importantly, average controllability of the left IFG pars opercularis was the best predictor among all 106 candidate predictors for treated naming recovery six months after treatment. Thus, average controllability of the left IFG pars opercularis outperformed traditional measures of regional lesion burden, total lesion burden, graph theory features, as well as demographic characteristics and baseline aphasia severity.

Previous research identifying the left IFG pars opercularis as a hub region in the residual language network after a left-hemispheric stroke (Fridriksson et al., 2018b). Moreover, Fridriksson et al. (2018b) show that damage to hub regions affects language performance of individuals with aphasia at least six months after their stroke and speculated that damage to these regions may have long-term consequences for communication abilities. Here, our findings indicate that integrity of the left IFG pars opercularis and its ability to support brain state transitions is relevant for recovery (Karrer et al., 2020).

The literature on controllability and language in general (outside of aphasia) is still relatively limited, but a recent study supports our findings of the crucial role of the IFG from an NCT perspective. Medaglia et al. (2018) examined the effects of TMS on language performance in healthy adults. The effects of TMS, applied over the left IFG, on the participants' performance in open response (sentence completion, verb generation) and closed response tasks (number naming) was dependent on different controllability features of the IFG. TMS-induced changes in open response tasks were associated with the IFG's controllability of communication between brain modules, while changes in closed response tasks were associated with the IFG's ability to control brain states.

Stroke lesion and regional controllability

In this study, we observed that the relationship between stroke lesions and regional controllability was not consistent, highlighting the importance of using NCT and not relying on lesion characteristics alone. Figure 6 provides an overview of the relationship between lesion locations, regional controllability, and graph theory measures.

One example for lesion locations impacting regional controllability measures is the MOG. The MOG had the highest average controllability across our participant cohort which would be a surprising result in a cohort of healthy individuals. However, given that our participants had strokes in the anterior brain circulation, thus the likelihood of damage to the MOG and/or its vicinity was low. As demonstrated in Figure 2, the MOG had a lower probability of lesion compared with other brain areas. Thus, control input injected into the MOG has a higher likelihood of resulting into a distributed response of the language system, given the preservation of the area. It should be noted that the MOG was not associated with recovery, hence the specificity of controllability in core language related areas in relationship with language outcomes.

While the lesion significantly affected the degree of controllability of some regions, it did not affect that of others. For example, average controllability of the left IFG pars opercularis was correlated with total brain lesion volume, and lesion volume of the left IFG pars opercularis itself. The larger the lesion, the lower the ability of the left IFG pars opercularis to spread and amplify control input through the network. In contrast, regional and total brain lesion volume were not associated with modal controllability of the anterior insula. Both regions, left IFG pars opercularis and anterior insula, were among the most commonly lesioned regions across all participants, with an average regional lesion volume of 53.8% (SD 39.1%) and 55.2% (SD 40.8%), respectively. This finding is expected since aphasia is typically the result of left

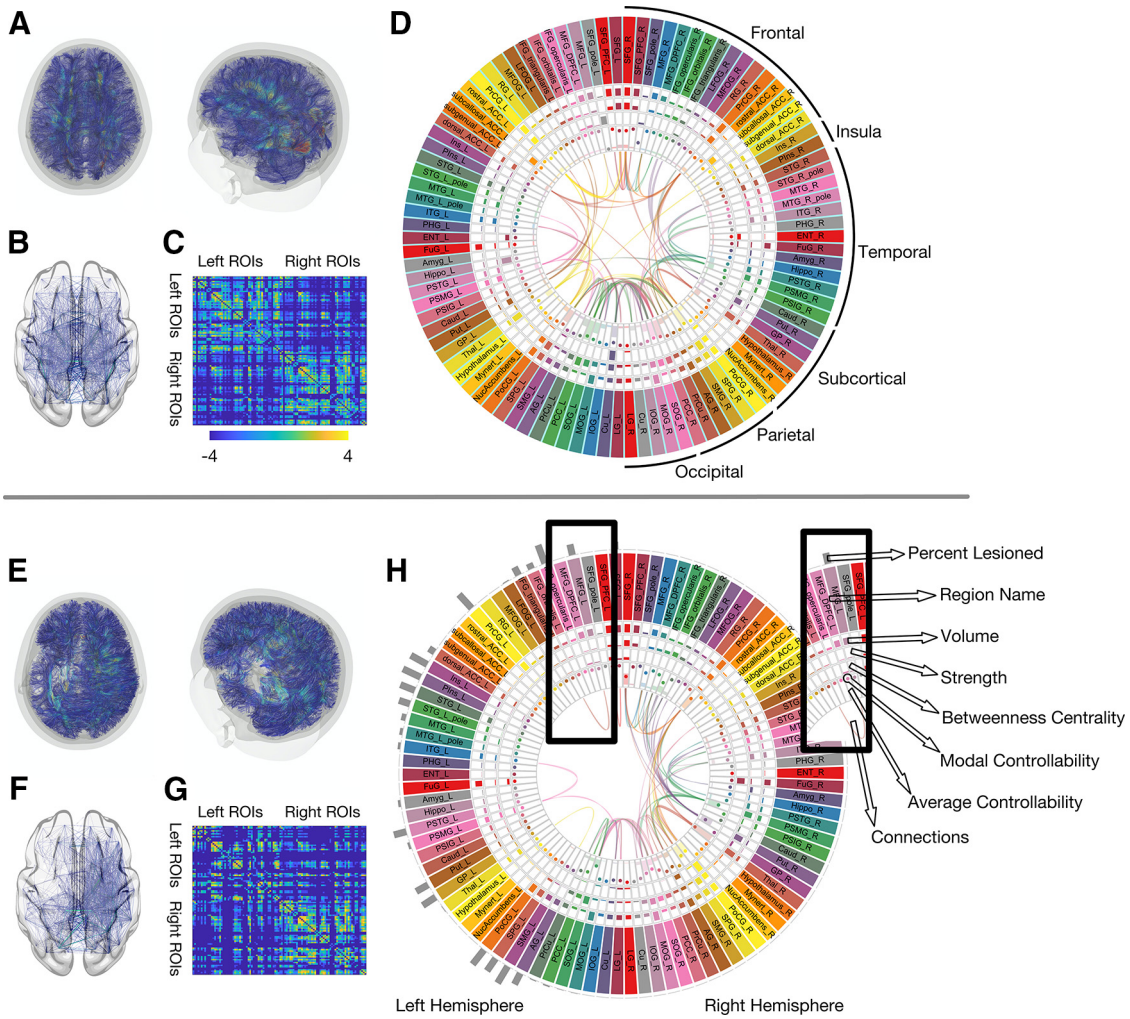

Figure 6. The impact of the stroke lesion on global and regional connectome measures. This composite figure provides a comprehensive visual summary of how a stroke lesion affects the structural connectome and its properties. For comparison, the average connectome data from 60 healthy individuals with the same demographic and risk factor profile (described previously; Marebwa et al., 2018) is shown in the upper panel (above the horizontal gray lone). Data from one participant with aphasia (lesion volume: 266 ml) in the lower panel. ***A***, ***E***, Reconstructed white matter fibers, here for visualization purposes based on deterministic tractography. ***B***, ***F***, Edges between gray matter regions from the JHU anatomic atlas. ***C***, ***G***, Adjacency matrices representing probabilistic streamlines between each region pair (color bar represent log values for better visualization). ***D***, ***H***, All structural connectome measures used in the analyses of this study: average controllability, modal controllability, regional lesion volume, node strength, and betweenness centrality, each one within a "track" of the figure, as indicated by the inset. Each box represents one gray matter region (for full region names, see Table 1). For visualization purposes, 98 of the included 104 gray matter regions are displayed here.

middle cerebral artery strokes. The reason why the regional lesion volume has no effect on the insula's modal controllability in our study remains a matter of speculation. It is possible that structural connections driving the insula's modal controllability are located more distant from the lesion core, and thus less likely to be damaged by the average stroke lesion location.

It is also possible that white matter health outside the stroke lesion impacts the relationship between network properties and NCT. The relationship between NCT and brain health may be a promising future new avenue of inquiry.

Limitations

This study did not assess the states that a network can transition to (for example, brain activation patterns) and their relationships with language. Instead, this study focused on the necessary and important task of clarifying whether NCT tools can be applied to poststroke networks, and if such a theoretical approach can be used to disclose aspects of network topology with clinical relevance, i.e., useful to predict clinical outcomes. We limited our analyses of regional controllability to 20 regions in the left hemisphere commonly associated with language processing. It remains to be investigated whether controllability of other regions has an impact on treated aphasia recovery. Further, while we examined controllability of the entire residual brain, future studies may address sub-network controllability (i.e., constrained to the language network).

Another limitation is that we leveraged data from an RCT assessing effects of tDCS on treated aphasia recovery. To account for potential effects related to tDCS, we included tDCS as a control variable in the regression models where tDCS presented as a nonsignificant predictor. Further, based on visual comparisons, the locations of the tDCS anode were different from the location of the identified ROIs in our study: the tDCS location was typically over the left parietal or left posterior temporal cortices (Fridriksson et al., 2018a), whereas the identified ROIs in this study are in the frontal lobe (IFG pars opercularis, IFG pars orbitalis) and anterior insula. Last, we performed Wilcoxon signed-rank test to determine differences between participants who received active tDCS and participants who received S-tDCS for average controllability of the left IFG pars opercularis, modal

controllability of the left IFG pars orbitalis, and modal controllability of the left anterior insula. There were no significant differences between these two groups for any measure ($p > 0.05$). Thus, while we cannot exclude overall effects of tDCS in our study, the likelihood that tDCS interfered with our results of regional controllability appear low.

In conclusion, topological properties of the residual networks, quantified from an NCT standpoint, are associated with aphasia recovery. The modal controllability of IFG pars opercularis is predictive of long-term treatment-related language improvement. Overall, NCT properties are not fully explained by the lesion and they are not directly associated with graph theoretical properties, and therefore provide another important window into the neurobiology of language. Stroke-related NCT measures provide a principled approach to evaluate the status of the residual language network and its interaction with the remaining brain network. This NCT approach may also disclose properties related to brain topology and brain health, from the perspective of white matter network integrity, which may guide future translational studies on the topic.

References

Andersson JLR, Sotiropoulos SN (2016) An integrated approach to correction for off-resonance effects and subject movement in diffusion MR imaging. Neuroimage 125:1063–1078.

Baldo JV, Arévalo A, Patterson JP, Dronkers NF (2013) Grey and white matter correlates of picture naming: evidence from a voxel-based lesion analysis of the Boston Naming Test. Cortex 49:658–667.

Behrens TEJ, Berg HJ, Jbabdi S, Rushworth MF, Woolrich MW (2007) Probabilistic diffusion tractography with multiple fibre orientations: what can we gain? Neuroimage 34:144–155.

Bernhardt BC, Fadaie F, Liu M, Caldairou B, Gu S, Jefferies E, Smallwood J, Bassett DS, Bernasconi A, Bernasconi N (2019) Temporal lobe epilepsy: hippocampal pathology modulates connectome topology and controllability. Neurology 92:e2209–e2220.e9.

Bonilha L, Gleichgerrcht E, Fridriksson J, Rorden C, Breedlove JL, Nesland T, Paulus W, Helms G, Focke NK (2015) Reproducibility of the structural brain connectome derived from diffusion tensor imaging. PLoS One 10: e0135247.

Bonilha L, Gleichgerrcht E, Nesland T, Rorden C, Fridriksson J (2016) Success of anomia treatment in aphasia is associated with preserved architecture of global and left temporal lobe structural networks. Neurorehabil Neural Repair 30:266–279.

Bonilha L, Rorden C, Fridriksson J (2014a) Assessing the clinical effect of residual cortical disconnection after ischemic strokes. Stroke 45:988–993.

Bonilha L, Nesland T, Rorden C, Fillmore P, Ratnayake RP, Fridriksson J (2014b) Mapping remote subcortical ramifications of injury after ischemic strokes. Behav Neurol 2014:215380.

Brandes U (2001) A faster algorithm for betweenness centrality. J Math Sociol 25:163–177.

Dragoy O, Akinina Y, Dronkers N (2017) Toward a functional neuroanatomy of semantic aphasia: a history and ten new cases. Cortex 97:164–182.

Faria AV, Joel SE, Zhang Y, Oishi K, van Zjil PC, Miller MI, Pekar JJ, Mori S (2012) Atlas-based analysis of resting-state functional connectivity: evaluation for reproducibility and multi-modal anatomy-function correlation studies. Neuroimage 61:613–621.

Fridriksson J, Yourganov G, Bonilha L, Basilakos A, Den Ouden DB, Rorden C (2016) Revealing the dual streams of speech processing. Proc Natl Acad Sci USA 113:15108–15113.

Fridriksson J, Rorden C, Elm JJ, Sen S, George MS, Bonilha L (2018a) Transcranial direct current stimulation vs sham stimulation to treat aphasia after stroke: a randomized clinical trial. JAMA Neurol 75:1470–1476.

Fridriksson J, den Ouden DB, Hillis AE, Hickok G, Rorden C, Basilakos A, Yourganov G, Bonilha L (2018b) Anatomy of aphasia revisited. Brain 141:848–862.

Fridriksson J, Basilakos A, Stark BC, Rorden C, Elm JJ, Gottfried M, George MS, Sen S, Bonilha L (2019) Transcranial direct current stimulation to treat aphasia: longitudinal analysis of a randomized controlled trial. Brain Stimul 12:190–191.

Gajardo-Vidal A, Lorca-Puls DL, Team P, Warner H, Pshdary B, Crinion JT, Leff AP, Hope TMH, Geva S, Seghier ML, Green DW, Bowman H, Price CJ (2021) Damage to Broca's area does not contribute to long-term speech production outcome after stroke. Brain 144:817–832.

Gilmore N, Meier EL, Johnson JP, Kiran S (2019) Nonlinguistic cognitive factors predict treatment-induced recovery in chronic poststroke aphasia. Arch Phys Med Rehabil 100:1251–1258.

Gleichgerrcht E, Fridriksson J, Rorden C, Bonilha L (2017) Connectome-based lesion-symptom mapping (CLSM): a novel approach to map neurological function. Neuroimage Clin 16:461–467.

Gross L (2008) From structure to function: mapping the connection matrix of the human brain. PLoS Biol 6:e164.

Gu S, Pasqualetti F, Cieslak M, Telesford QK, Yu AB, Kahn AE, Medaglia JD, Vettel JM, Miller MB, Grafton ST, Bassett DS (2015) Controllability of structural brain networks. Nat Commun 6:8414.

Gu S, Betzel RF, Mattar MG, Cieslak M, Delio PR, Grafton ST, Pasqualetti F, Bassett DS (2017) Optimal trajectories of brain state transitions. Neuroimage 148:305–317.

Hagmann P, Cammoun L, Gigandet X, Meuli R, Honey CJ, Wedeen VJ, Sporns O (2008) Mapping the structural core of human cerebral cortex. PLoS Biol 6:e159.

Hernández M, Guerrero GD, Cecilia JM, García JM, Inuggi A, Jbabdi S, Behrens TEJ, Sotiropoulos SN (2013) Accelerating fibre orientation estimation from diffusion weighted magnetic resonance imaging using GPUs. PLoS One 8:e61892.

Karrer TM, Kim JZ, Stiso J, Kahn AE, Pasqualetti F, Habel U, Bassett DS (2020) A practical guide to methodological considerations in the controllability of structural brain networks. J Neural Eng 17:026031.

Kertesz A (2007) The Western aphasia battery - revised. New York: Grune and Stratton.

Kristinsson S, Basilakos A, Elm J, Spell LA, Bonilha L, Rorden C, den Ouden DB, Cassarly C, Sen S, Hillis A, Hickok G, Fridriksson J (2021) Individualized response to semantic versus phonological aphasia therapies in stroke. Brain Commun 3:fcab174.

Lambon Ralph MA, Snell C, Fillingham JK, Conroy P, Sage K (2010) Predicting the outcome of anomia therapy for people with aphasia post CVA: both language and cognitive status are key predictors. Neuropsychol Rehabil 20:289–305.

Li X, Morgan PS, Ashburner J, Smith J, Rorden C (2016) The first step for neuroimaging data analysis: DICOM to NIfTI conversion. J Neurosci Methods 264:47–56.

Lidzba K, Staudt M, Zieske F, Schwilling E, Ackermann H (2012) Prestroke/poststroke fMRI in aphasia: perilesional hemodynamic activation and language recovery. Neurology 78:289–291.

Marebwa BK, Adams RJ, Magwood GS, Basilakos A, Mueller M, Rorden C, Fridriksson J, Bonilha L (2018) Cardiovascular risk factors and brain health: impact on long-range cortical connections and cognitive performance. J Am Heart Assoc 7:e010054.

McKinnon ET, Fridriksson J, Glenn GR, Jensen JH, Helpern JA, Basilakos A, Rorden C, Shih AY, Spampinato MV, Bonilha L (2017) Structural plasticity of the ventral stream and aphasia recovery. Ann Neurol 82:147–151.

Medaglia JD, Harvey DY, White N, Kelkar A, Zimmerman J, Bassett DS, Hamilton RH (2018) Network controllability in the inferior frontal gyrus relates to controlled language variability and susceptibility to TMS. J Neurosci 38:6399–6410.

Meier EL, Johnson JP, Pan Y, Kiran S (2019) The utility of lesion classification in predicting language and treatment outcomes in chronic stroke-induced aphasia. Brain Imaging Behav 13:1510–1525.

Meinzer M, Elbert T, Wienbruch C, Djundja D, Barthel G, Rockstroh B (2004) Intensive language training enhances brain plasticity in chronic aphasia. BMC Biol 2:20.

Mirman D, Chen Q, Zhang Y, Wang Z, Faseyitan OK, Coslett HB, Schwartz MF (2015) Neural organization of spoken language revealed by lesion-symptom mapping. Nat Commun 6:6762.

Nachev P, Coulthard E, Jäger HR, Kennard C, Husain M (2008) Enantiomorphic normalization of focally lesioned brains. Neuroimage 39:1215–1226.

Parkes L, Moore TM, Calkins ME, Cieslak M, Roalf DR, Wolf DH, Gur RC, Gur RE, Satterthwaite TD, Bassett DS (2020) Network controllability in

transmodal cortex predicts psychosis spectrum symptoms. medRxiv 2020.2010.2001.20205336.

Pustina D, Coslett HB, Ungar L, Faseyitan OK, Medaglia JD, Avants B, Schwartz MF (2017) Enhanced estimations of post-stroke aphasia severity using stacked multimodal predictions. Hum Brain Mapp 38:5603–5615.

Reese TG, Heid O, Weisskoff RM, Wedeen VJ (2003) Reduction of eddy-current-induced distortion in diffusion MRI using a twice-refocused spin echo. Magn Reson Med 49:177–182.

Roach A, Schwartz MF, Martin N, Grewal RS, Brecher A (1996) The Philadelphia Naming Test: scoring and rationale. Clin Aphasiol 24:121–133.

Rorden C, Bonilha L, Fridriksson J, Bender B, Karnath HO (2012) Age-specific CT and MRI templates for spatial normalization. Neuroimage 61:957–965.

Rubinov M, Sporns O (2010) Complex network measures of brain connectivity: uses and interpretations. Neuroimage 52:1059–1069.

Shain C, Blank IA, van Schijndel M, Schuler W, Fedorenko E (2020) fMRI reveals language-specific predictive coding during naturalistic sentence comprehension. Neuropsychologia 138:107307.

Stockert A, Wawrzyniak M, Klingbeil J, Wrede K, Kümmerer D, Hartwigsen G, Kaller CP, Weiller C, Saur D (2020) Dynamics of language reorganization after left temporo-parietal and frontal stroke. Brain 143:844–861.

Turken AU, Dronkers NF (2011) The neural architecture of the language comprehension network: converging evidence from lesion and connectivity analyses. Front Syst Neurosci 5:1.

Wade DT, Hewer RL, David RM, Enderby PM (1986) Aphasia after stroke: natural history and associated deficits. J Neurol Neurosurg Psychiatry 49:11–16.

Wilmskoetter J, Fridriksson J, Gleichgerrcht E, Stark BC, Delgaizo J, Hickok G, Vaden KI Jr, Hillis AE, Rorden C, Bonilha L (2019a) Neuroanatomical structures supporting lexical diversity, sophistication, and phonological word features during discourse. Neuroimage Clin 24:101961.

Wilmskoetter J, Marebwa BK, Basilakos A, Fridriksson J, Rorden C, Stark BC, Johnson L, Hickok G, Hillis AE, Bonilha L (2019b) Long-range fibre damage in small vessel brain disease affects aphasia severity. Brain 142:3190–3201.

Xing S, Lacey EH, Skipper-Kallal LM, Zeng J, Turkeltaub PE (2017) White matter correlates of auditory comprehension outcomes in chronic post-stroke aphasia. Front Neurol 8:54.

Zou H, Hastie T (2005) Regularization and variable selection via the elastic net. J R Stat Soc B 67:301–320.